12th International Conference on Contact Mechanics and Wear of Rail/Wheel Systems (CM2022), Melbourne, Australia, 4-7 September 2022

SMOOTH TRANSITION INSULATED RAIL JOINTS

Gianluca Megna [1,*], Andrea Bracciali [1]

[1] Department of Industrial Engineering, Università degli Studi di Firenze, Italy

[*] E-mail: gianluca.megna@unifi.it

Abstract: Insulated Railway Joints fail mainly because of repeated shocks in the end post region causing loss of insulation (lipping) and eventually leading to broken rails and train derailments. Qualification tests are inadequate as they do not replicate impact loads. A patented joint named ABJ, made of switch rails forged with a very shallow inclined cut and a thick cover joint, is introduced in the paper. ABJ shows no dip angle in the transition area, resulting is smooth wheel-rail transition forces preventing rail damage, impact noise, vibrations and ballast deterioration. It can be installed on standard track and it is tampable.

Keywords: Insulated Rail Joints, wheel-rail impacts, track loading, joint failures, railway noise, derailment.

1. Introduction

Continuously welded rail (CWR) is widespread in railway tracks and the need of joints has been significantly reduced over the years. However, electrically insulated joints for signalling purpose, i.e. Insulated Rail Joints (IRJ), still survive as they are required to define track circuits.

Conventional IRJ require a "square" (90°) cut preparation of two rails, then the gap is filled with a 5 mm-nylon slice, called "end post", and the rails are connected using fishplates and fishbolts. The gap leads to a reduction of the stiffness properties compared to plain rail that generates a dip angle leading to shocks which reduce expected service life from 12 to 18 months [1]. Because of shocks, large impulse noise peaks [2] and high dynamics forces [3] are generated at each wheel passing, causing vibrations and damaging ballast. Shocks ultimately results in joint failure with different modes, including plastic flow and eventually to the contact of rail ends, vanishing the required insulation of the joint and increasing the maintenance costs [4].

Cracks may even progress until portions of the rails are detached. This was the main cause of the accident in Pioltello (Milan, Italy) on 25 January 2018, which left three people dead and many injured. Although so-called "star cracks", i.e. cracks starting at 45° from the bolt holes (defect 135 according to code UIC 712 on rail defects), can be greatly reduced by the "cold bolt expansion" technique, nothing can be done on impacts in the end post area.

Some IRJ design dates back to the '60s. In order to reduce as much as possible the risk of failures, wide sleepers were developed to better support the joint and a range of transducers (passive, electrical, optical) was developed to tackle any joint ungluing and gap widening. None of these measures cures the problem, and better NDT (ultrasonic) techniques can only intercept cracks before they reach a critical size.

Attempts to improve the mechanical behaviour of IRJ were made without definitive results. A parametric study including different track configurations [5] shows that stresses in rail head are not significantly affected by track stiffness, by the IRJ position (suspended or hanging) or by the shape, i.e. the stiffness, of the fishplates. External reinforcements were studied to reduce joint deflection [6], while railhead shape optimization to reduce stress levels was simulated [7] and tested [8]. The concept of a sleeper embedded joint is shown in [9].

The most obvious solution to reduce impacts, that is the use of an inclined cut between the rails to perform a progressive transition, can be implemented with important limitations due to the limited rail web thickness. The angle of the cut was found to be between 60° and 75°, such that the resulting transition is too short to avoid high stresses. The behaviour of a standard 90° cut joint and a 75° cut joint was evaluated in [10], showing that there are not major advantages in using the inclined cut.

The first option to "artificially" increase the web width is to laterally bend standard rails that were used in the past for expansion joints. Machining of the bent rails is then needed to restore the original railhead shape. An example of such expansion joint will be shown later (see Figure 19), but to authors' knowledge no IRJ was produced by using this solution.

Another possibility to create a longer ("scarf" or "mitre") cut is to machine special rails with thicker web used for bridge expansion joints. The authors of paper [11] concluded anyway that the solution was too expensive for ordinary joints. Moreover, only the static performances of the joint were evaluated and a detailed analysis of the wheel-joint interaction was not found in the literature.

This paper introduces a fishplate-free innovative joint, called ABJ, characterized by a very shallow (<3°) tapered cut and a stiff thick joint cover. The aim is to compare the ABJ and conventional IRJ wheel-rail interaction features,

validating the principle that a progressive and smooth transition leads to enormous advantages in terms of joint integrity and service life.

2. Description of ABJ

The proposed joint, called ABJ, (Figure 1, Figure 2), is patent pending [13]. It can be assembled starting from standard components with limited machining operations and with manufacturing sequences that are very similar to conventional IRJ.

An ABJ is made from two commercially available forged and machined switch rails (e.g. 60E1A2 [14]). The use of switch rails with thicker web (40 mm) and smaller height (134 mm) than a standard 60E1 rail allows to get the following advantages:

- a long <3° cut, obtained by forging, replaces the 90° cut of standard IRJ, resulting in a "smooth" transition about 500 mm long;
- a stiffening plate (joint cover) is connected under the switch rails foot resulting in a continuously supported joint with high bending stiffness;
- conventional IRJ fishplates are suppressed, freeing the area below the railhead for tampers rail lifting units;
- the joint cover is machined to accommodate standard rail fasteners (and therefore sleepers);
- the length and the geometry of the joint are such that the sleeper spacing is unchanged;
- use of advanced insulating material led to reduce hole size, allowing a larger number of bolts if needed;
- the number of bolts is arbitrary and can be either even or odd according to the design specifications.

The application of two ABJ to a track section is shown in Figure 3. Due the aforementioned properties, installation is straightforward and track maintenance is hassle-free.

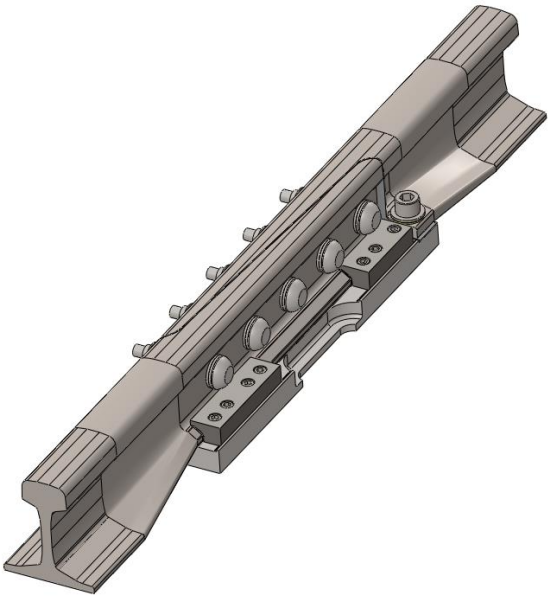

Figure 1. *CAD model of a "heavy" version of ABJ*

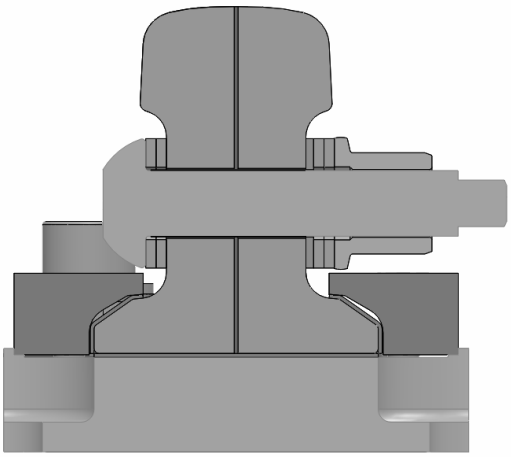

Figure 2. *Cross section of the ABJ in the transversal midplane. The absence of the fishplates show that tamping machines can lift the track without interruption. The joint is seen as a plain track from the maintenance point of view.*

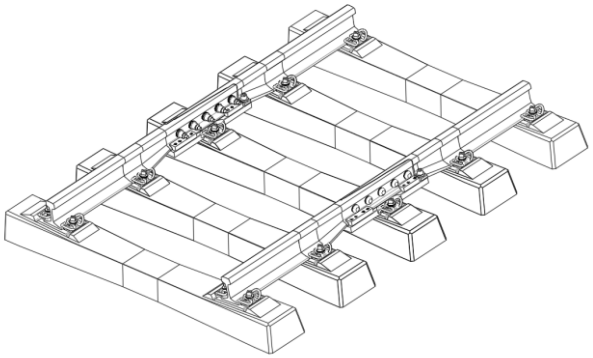

Figure 3. *Short track panel view including two ABJ (rail welds not shown). Standard rail fastening systems and standard sleepers can be used. Sleeper spacing is unchanged.*

The two switch rails are glued to each other with an insulating fiberglass layer in between and connected by five lockbolts with thin insulating short tubes made of advanced polymers. This assembly is then glued and bolted to the lower plate with another insulating layer in between. Further locking elements may be added, if needed, and they are clearly visible in Figure 1.

ABJ has a highly modular, as the number of lockbolts, the length of the stiffening plate and its connection to the rails can be adapted to specific needs. As an example, underground metro tracks are subjected to lower mechanical and thermal stresses, and "light" versions of ABJ are available.

Although of low interest in the present context, accurate structural validations were performed by fully non-linear a FEA model, including lockbolts pretensioning and considering mechanical properties of high strength epoxy glue and insulating layers (Figure 4).

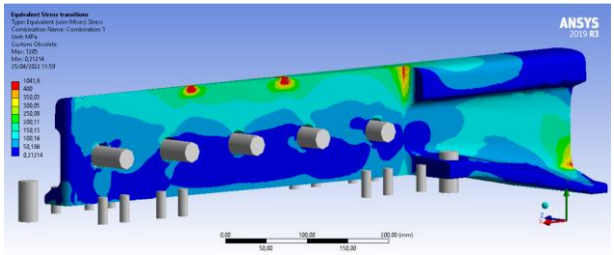

Figure 4. *Example of ABJ FEA modelling (fatigue bending stresses on a switch rail). The "red stress dots" on the upper surface are due to the local effect of the applied vertical forces.*

3. Contact mechanics of IRJ/ABJ

Numerical analyses such as finite element (FEA) and multibody (MBA) are extensively used for the assessment of the mechanical behaviour or railway components.

FEA is mainly used to calculate stresses and strains in IRJ due to multi-axial loading conditions at the wheel-rail contact, studying the effects of different parameters on rolling contact fatigue and plastic deformation at the rail head. FEA in combination with material constitutive models can predict localized ratcheting, or lipping, of the rail edge at the end post location [15] [16].

The bending stiffness discontinuity in a conventional IRJ can be idealized as a dip angle irregularity, which generates impact forces (P_1) and low frequencies forces (P_2) greater than the static force (P_0) when the vehicle runs on it. The effect of this irregularity can be evaluated by means of two-dimensional or three-dimensional models of the vehicle-track interaction in the presence of joints.

A three-dimensional model is presented in [17] with the aim to develop a simplified equation for impact forces prediction. The resulting forces (P_1=1.05÷1.66 P_0, P_2=1.03÷1.30 P_0), that depend on the vehicle speed (v=25÷100 km/h) and on the dip angle of the irregularity (α=0.8÷2.4 mrad), are therefore compared to the analytical formulation from [18].

A parametric study of the vehicle-track interaction using a two-dimensional model is described in [19], showing that the P_1 force also depends on the shape of the irregularity and not only on the value of the joint angle. Nevertheless, unsprung mass and joint angle are the main parameters influencing the impact force. It results that the impact force cannot be eliminated by working on the current geometry of IRJ.

3.1. Model description and tuning

Both static and dynamic non-linear FEA models of ABJ and IRJ were developed to investigate and compare their behaviour. The FEA model (Figure 5, Figure 6) uses 3D elements for the central part that includes the detailed joint geometry and 1D beam elements for the external parts. The rail is supported by spring elements with a vertical stiffness of k_z=20 kN/mm simulating the influence of both the railpad and the ballast.

Table 1. *Main characteristics of FEA models*

	IRJ	ABJ
Total length of the model [m]	9.0	9.6
Solid model length [m]	3.0	3.6
Number of supporting elements [-]	16	17

The model for the static analysis considered loads directly applied on the rail, while in the dynamic analyses a load of 98.1 kN (10 t wheel load) was applied by 1/2 of wheelset mass (unsprung mass = 750 kg), 1/4 of bogie mass (simply sprung mass = 2000 kg) and 1/8 of carbody mass (double sprung mass = 7250 kg). These parameters are typical of an 80 t locomotive, with two bogies with a mass of 11 t each.

A 940 mm diameter wheel was modelled to generate the wheel-rail contact, with a friction coefficient f=0.3. The masses are connected by a primary spring with a stiffness k_p=1000 N/mm and a secondary spring with a stiffness of k_s=450 N/mm. The rail 60E1 has an inclination of 1:20, while the wheel has a simplified conical profile.

Contact stress analysis was performed by finely meshing the bodies at the wheel-rail contact position for the dynamic analysis (Figure 5), with the aim to reproduce the Hertzian contact in the static position. The accuracy of the model was checked by comparing numerical results of the contact pressure distribution with Hertz theory (1), where p_0 (2) is the maximum Hertzian pressure, a and b are the semi-axes of the elliptic contact area in the x (rolling) and y (transverse) directions and N is the normal load. The semi-axes can be calculated by means of look-up tables or in closed form according to [20].

$$p = p_0 \left(1 - \left(\frac{x}{a}\right)^2 - \left(\frac{y}{b}\right)^2\right)^{1/2} \quad (1)$$

$$p_0 = \frac{3N}{2\pi ab} \quad (2)$$

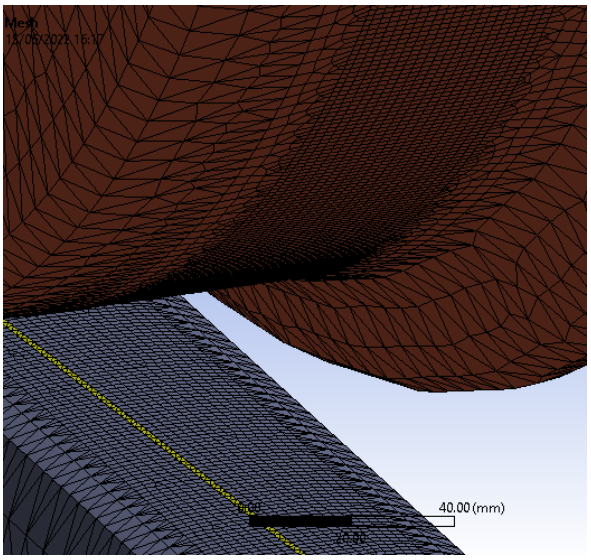

Figure 5. *Detail of the mesh at the wheel rail contact for the ABJ (the yellow strip being the insulating fiberglass sheet separating the switch rails).*

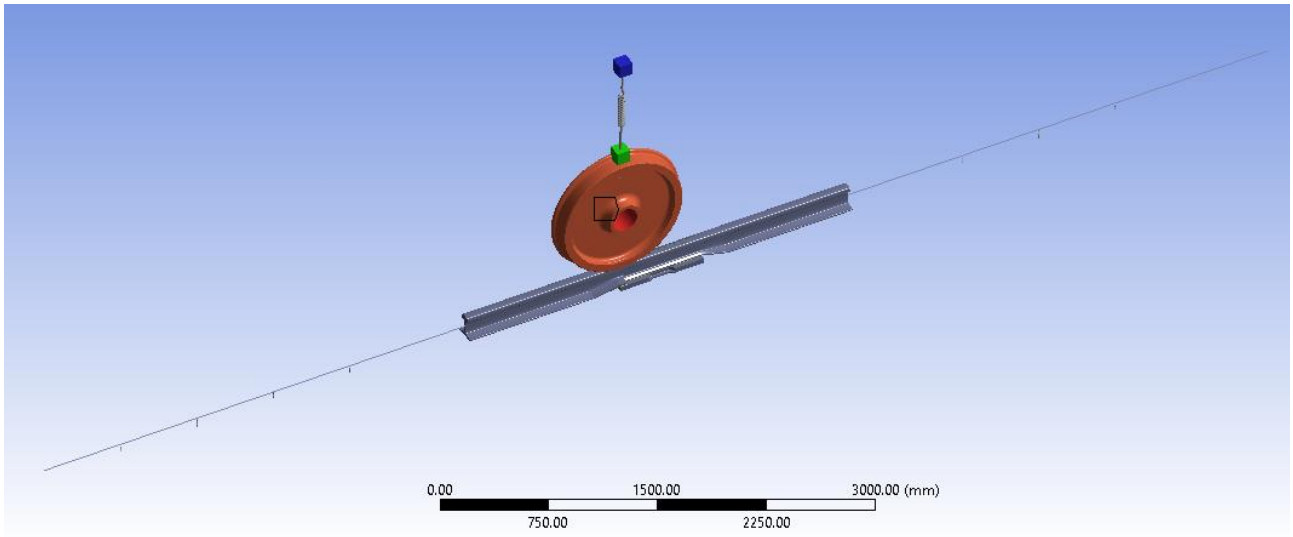

Figure 6. *FEA model of the ABJ. The green and the blue blocks represent the bogie mass and the carbody mass respectively. In this frame the wheel is entering the ABJ with the prescribed speed.*

A test load of 100 kN resulted in p_0=1190 MPa, a=7.6 mm and b=5.3 mm. Figure 7 shows that smaller element sizes provide a better agreement with Hertz's theory. Cubic elements with 2 mm edge size were chosen as they resulted in an error of 2.5% in terms of maximum contact pressure.

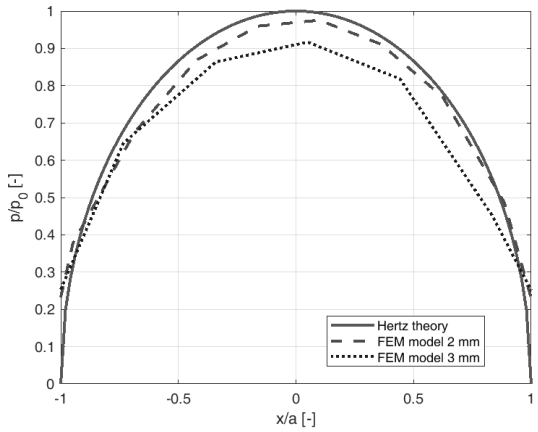

Figure 7. *Contact pressure distribution along the longitudinal axis from Hertz theory and FEA model with different of element size for meshing*

3.2. Static behaviour

The IRJ was simulated in a common condition for this kind of joint, i.e. with the joint *suspended* (midplane x=0 coincident with the midspan of the sleepers), while the ABJ was simulated in its design condition, i.e. *supported* by a sleeper (midplane x=0 over the sleeper). Both models were subjected to an exceptional static vertical load of 200 kN applied in the midplane x=0.

While the stiffness of IRJ at the end post is much lower than that of the rail, the ABJ shows a more uniform stiffness along the entire transition. Table 2 shows the comparison of rail deflection for both the joints, while the cross-section moment of inertia J_{yy} along the axis of the joint can be seen in Figure 8. Rail deflection of both types of joint is shown in Figure 9.

Table 2. *Static deflection and static stresses of IRJ and ABJ in the midplane (x=0) of the joint under a point exceptional load of 200 kN*

Parameter	IRJ	ABJ
Vertical deflection	-2.73 mm	-2.47 mm
Maximum Von Mises stress	318 MPa	102 MPa

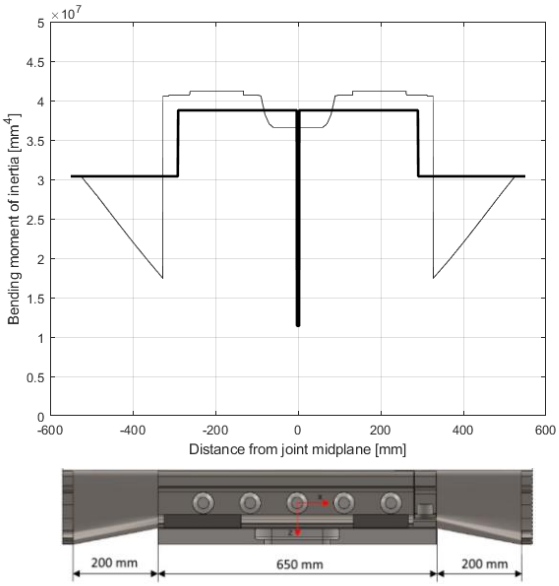

Figure 8. *Moment of inertia of IRJ (thick line) and ABJ (thin line) along the joint axis. The overall length of the joint (1050 mm) is limited by the constrain of using standard sleepers at both ends.*

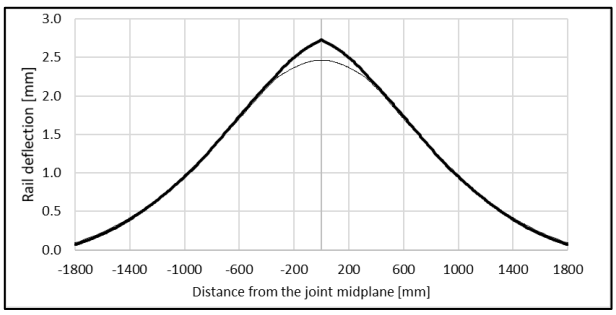

Figure 9. *Rail deflection of IRJ (thick line) and ABJ (thin line) under a 200 kN load applied at the centre of the joint.*

Not surprisingly, the ABJ provides a deflection that is only 4% smaller than the IRJ one. This may be justified considering that deflection is related to the double integral of the $M(x)/EJ(x)$ and it is affected in a limited way by local large stiffness variations. Similarly, ABJ limited and smooth reduction of stiffness in the forged transition leads to a negligibly greater rail deflection under wheel loads. It may be concluded that acting on joint stiffness leads to only limited advantages.

The most important feature exhibited by the ABJ is the absence of the dip in the end post area of IRJ (α=1.6 mrad for the present case). Angles of deformation are the first integral of the $M(x)/EJ(x)$ and are much more sensitive to local $J(x)$ large variations.

About external stresses (not related to fasteners preloading), maximum stresses appear in the fishplates for the IRJ while in the ABJ they are in the joint cover with values very close to (or even slightly smaller than) those for the plain rail (in the order of 105 MPa over a sleeper) when the joint is centrally loaded.

A further analysis was conducted by slowly moving the load along the model, analysing stresses and comparing deflections with those appearing over a sleeper (1200 mm and 900 mm respectively for IRJ and ABJ) in the standard track (Figure 10). For IRJ, the maximum stress was found in the fishplates when the load is applied between 0 and 200 mm.

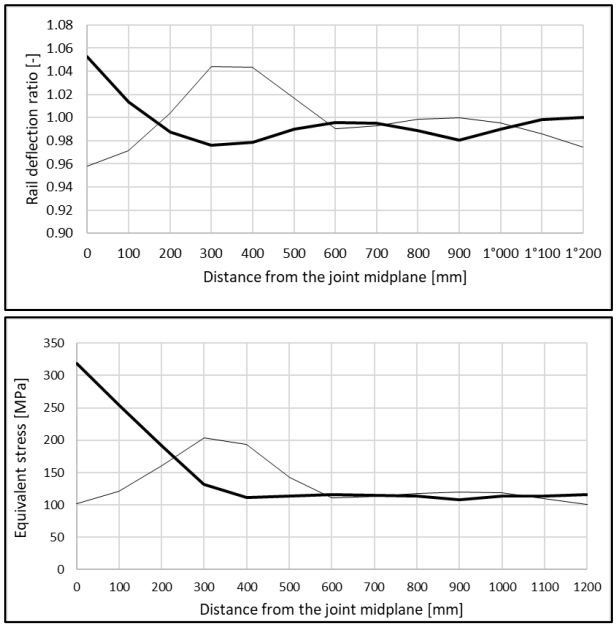

Figure 10. *Ratio of the point vertical rail deflection and the plain rail deflection for IRJ (thick line) and ABJ (thin line) under a slowly moving static load of 200 kN starting from x=0 (top). Maximum equivalent stresses according to Von Mises criterion (bottom).*

3.3. Dynamic behaviour of the IRJ

Fully transient dynamic analyses were performed with the vehicle model passing over the joint at constant speed (v=30.5 m/s=110 km/h) with an integration time step of 0.1 ms.

Rails generate a dip angle of 0.9 mrad (Figure 11) at the wheel passage over the midplane (x=0). Vertical displacement at the midplane is shown in Figure 12 as a function of the wheel position. Rail deformation initially increases while the wheel moves along the joint as the fishplates are not able to restore the correct geometry because of the gap.

The gap generates a wheel/rail unloading with a consequent upward rail movement that is evident at x=0 mm. Wheel-rail contact conditions (Figure 13) show the resulting impact force P_1. The peak value of the force is about 121 kN, which results in a DIF (Dynamic Impact Factor) of 1.23, a value that is comparable to those described in [17] for similar conditions. After the void, the joint is loaded again reaching the highest displacement about 180 mm after the joint while the vertical force increases again.

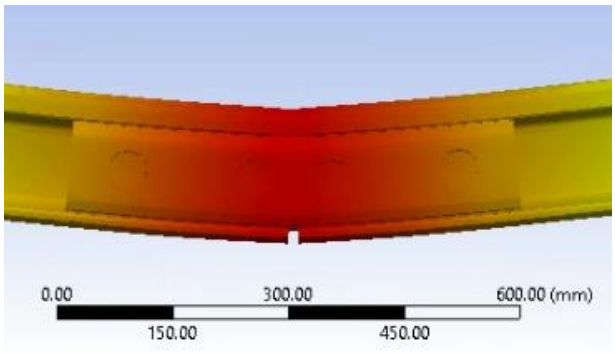

Figure 11. *100x magnification of the vertical deflection of the joint when the wheel passes at x=0.*

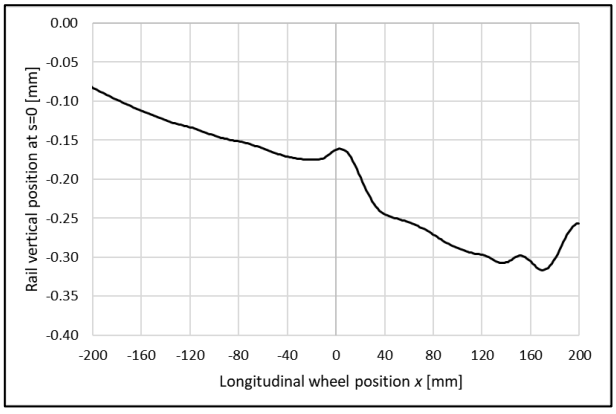

Figure 12. *Vertical displacement of IRJ at x=0 during wheel pass-by.*

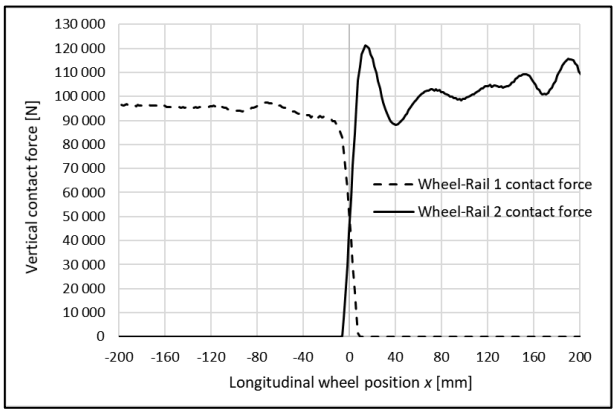

Figure 13. *Vertical contact force between the wheel and the two rails of IRJ during wheel pass-by.*

3.4. Dynamic behaviour of the ABJ

Shocks are completely avoided with the ABJ solution, for which the shallow transition results in a longer transfer of the load between the two rails. The contact patch is split between the two rails depending on the actual wheel and rail profile coupling but, in any case, it lasts for much longer than for any existing IRJ.

In nominal conditions (new wheels and new rails) the contact is centred. As shown in Figure 14 for an elliptical contact patch with a=7.6 mm, b=5.3 mm, the load transfer between the two rails is symmetrical w.r.t. the midplane of the joint and the length needed to complete the transition is about 200 mm. The contact patch is obviously equally shared by the two rails at x=0 mm. The transition length is around 13 times the longitudinal size of contact patch, while for square-cut or 45°-cut IRJ it is always shorter than the contact patch.

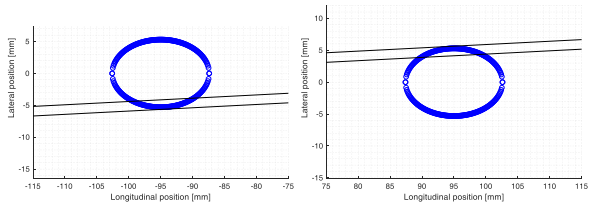

Figure 14. *Initial (left) and final (right) positions of the wheel-rail contact patch.*

Vertical displacement of the ABJ measured at the midplane x=0 mm (Figure 15) highlights the absence of any discontinuities during the wheel pass-by. This results in a nearly constant vertical force at the passage over the joint (Figure 16), that withstands a sort of "handover" process between the rails resulting in a quiet and extremely smooth passage of the wheel over the joint.

Figure 15. *Vertical displacement at the x=0 during wheel pass-by.*

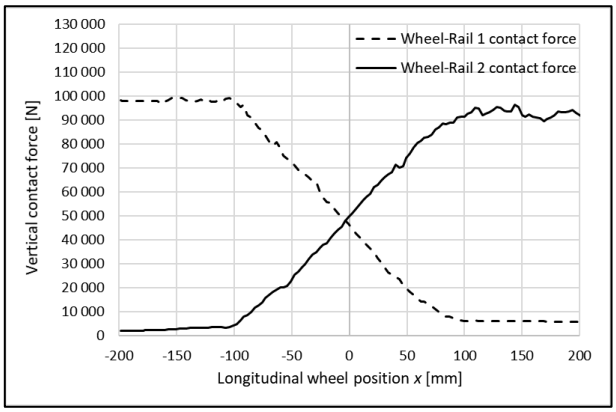

Figure 16. *Vertical contact force between the wheel and the two rails of ABJ during wheel pass-by.*

If the contact point between wheel and rail is laterally shifted due to worn profiles or different rail inclination, the transition is not symmetrical with respect to the midplane of the joint, the length needed to complete the load transfer between the two rails is shorter and the fillet at the end of the cut is involved. In the example shown in Figure 17 the transition length is about 60 mm.

Figure 18 shows that the transfer of the contact force between the rails is faster. Nevertheless, also in this case the transition is able to avoid impact forces and the wheel passage is much smoother than any IRJ.

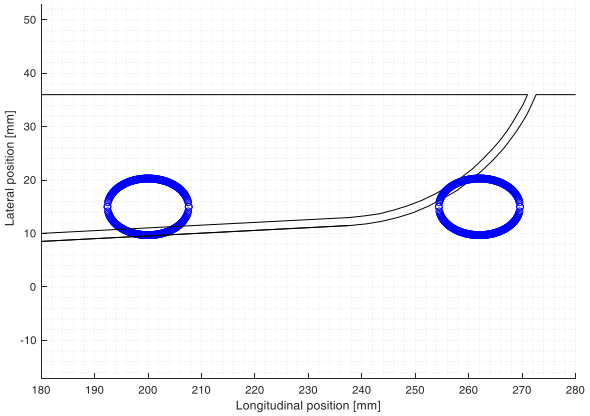

Figure 17. *Initial and final contact positions considering a 15 mm lateral shift of the wheel-rail contact.*

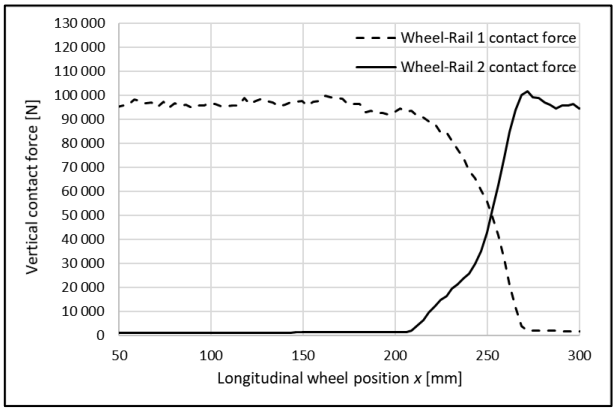

Figure 18. *Vertical contact force between the wheel and the two rails of ABJ during wheel pass-by in asymmetric conditions of the contact patch.*

4. Discussion of the results

The main results from the simulations say that the transition from one rail to the other is smooth for the ABJ and without the shocks typical of the conventional IRJ.

This is not surprising since there are at least two families of railway products that show some similarities with the ABJ. They are expansion joints, often used near steel bridges (Figure 19), and the switch rail / stock rail pair (Figure 21). For both these components damages are less frequent and much less catastrophic than for IRJ. This was justified by a large number of numerical studies (e.g. [21]).

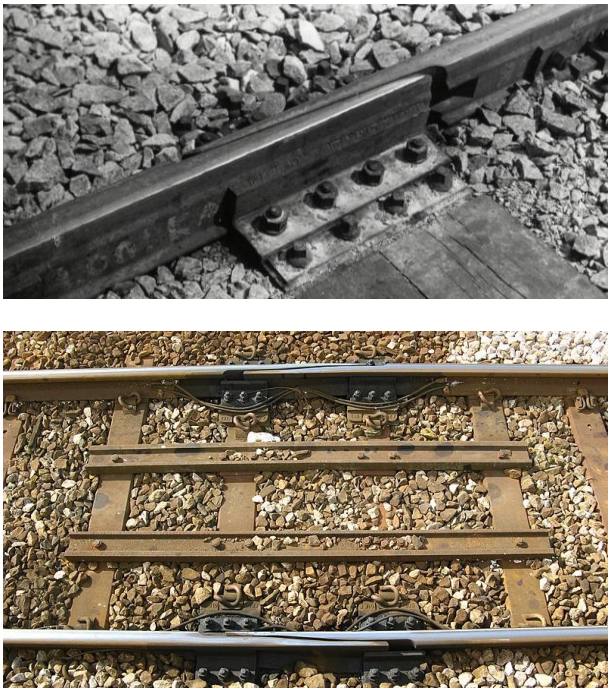

Figure 19. *Expansion joint samples (source: Internet)*

Figure 20. *Closed switch rail / stock rail pair of an old and heavily loaded turnout. The load transfer is smooth and no damages are visible*

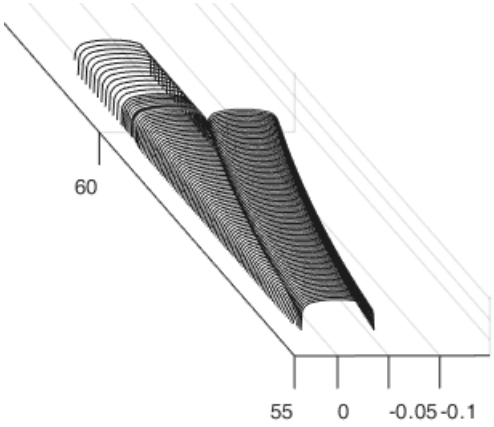

Figure 21. *Discretization of the transition area in a turnout (from [21])*

The main difference between ABJ and expansion joints/switch blades is that the latter are "movable" while the first is bolted and glued becoming a single body. This implies that in the ABJ there will be no relative movements between the rails and the joint cover, eliminating the already scarcely relevant damages occurring to expansion joints/switch blades.

It looks clear that any further investigation searching for plastic strains, damage and accumulation of deformation makes no sense as the root cause for these phenomena (shocks at wheel passing) simply does not exist.

5. Validation of the ABJ

Railway administrations and infrastructure manager published national technical specifications to check the "quality" of IRJ that they are purchasing.

An extensive comparison of these standards goes beyond the goal of this paper. A limited comparison of national specifications with the next European standard [12] highlights (Figure 23) that while some countries try to replicate the behaviour in service (in one case with two vertical actuators imposing a sort of "passing load") some others simply introduce conventional loads.

If axial loads are relatively easily estimated from thermal considerations, vertical testing loads are largely variable. This proves the inadequacy of any static testing layout to reliably assess the probability of survival of a joint when installed in real track subjected to impacts in the end post area.

All these tests are therefore useless to estimate the service life of a given joint, and only tests in a real environment may find whether a specific architecture is valid or not.

At the time of writing three prototypes (Figure 22) are going to be assembled to perform static (pull-apart) and fatigue test according to according to the European Standard prEN 16843:2019 [12] (that should be issued by August 2022) and to Italian requirements (that are more stringent); further tests will be made with the available equipment to assess the validity of the concept for heavy haul applications, although from a numerical point of

view all the testing specifications were already successfully checked.

Figure 22. *First prototypes of ABJ. Top: switch rails finished by milling. Bottom: assembly tests with dummy fastenings and insulating sheets.*

6. Conclusions and further developments

The concept of an innovative insulated rail joint made assembling standard rail components, named ABJ, was introduced in the paper. Extensive calculations showed the superiority of the ABJ compared to conventional insulated rail joints as the impact force, rail damages, failures, noise, vibrations and ballast degradation are all prevented. ABJ can be installed in any plain track with standard sleepers and standard rail fastening systems, allowing continuous track tamping.

At the moment of writing laboratory tests are planned to be concluded before the conference where they will be reported. Official homologation laboratory tests will immediately follow.

In the short term, line tests are already planned on a conventional line and on a heavy haul line to assess the actual behaviour of ABJ in service.

Acknowledgments
The contribution from the companies D.R. Ferroviaria Italiana s.r.l. (machining, assembling, testing), Dielettrika Ligure (fiberglass insulators) and Politubes s.r.l. (Mylar+Nomex insulator) is gratefully acknowledged.

Country	Standard	Static test force [kN]	Wheel load [kN]	Force [kN]	Joint support distance [mm]	Max bending [kNm]	# cycles [*10⁶]	Freq. [Hz]	Note
ITA	RFI TCAR SF AR 07 008 A	F_h=1500	N/A	F_v=30÷300	1100	*71.25*	2	3÷5	
EU	prEN 16843:2019	F_h=1450 [1]	125	F_v=*5÷167.6* [2]	924 ≤ Ls ≤ 1268 [3]	39.8 [4]	3	3÷10	
TUR	TCDD IRC: 2017	F_h=2000	N/A	F_v=15÷200	1000	*50*	5	≤ 20	
ESP	ET 03.360.109.7	F_h=1290	N/A	F_v=39.2÷172.87	640	*27.7* [5] (biaxial test)	3	6÷10	Hardened railhead ends
AUS	AS 1085.12-2002	F_h=1130 F_v=210 [6] (biaxial test)	N/A	F_v=1100 (static) [7] F_v=10÷245 (fatigue)[8]	600 (static) [9] 1100 (fatigue) [10]	*165* (static) *67.4* (fatigue)	3	5÷10	Hardened railhead ends
GBR	RT/CE/S/023 1996 [11]	F_h=700 (1 h)	N/A	F_v=5÷205 F_h=460 (const.)	1286 [12]	*46.5* [13]	2	1÷10	

[1] Calculated for a 60E1 rail, with ΔT=50 °C, safety coefficient γs=1.5.
[2] Calculated from Eqn. (9) with support distance L_s=1100 mm and longitudinal distance between vertical supports L_w=150 mm.
[3] Calculated for a typical fishplate with L_f=580 mm and a rail height of 172 mm with Eqn. (8).
[4] Taken from table G.1 (for a 60E1 rail, suspended joint, maximum vertical deflection of the track w_{max}=1.5 mm).
[5] A total of 1826 cycles of traction/compression are applied with -45/+45 kN (spring + autumn), -60/+30 kN (summer), -30/+60 kN (winter).
[6] For a 60 kg/m rail according to Table D1 (axial load 1280 kN and vertical load 300 kN for a 68 kg/m).
[7] Called "Load deflection test" with max deflection of 20 mm for 60 kg/m rail. It further requires reaching 1900 kN or failure.
[8] Fatigue load for 60 kg/m rail (10÷290 kN for 68 kg/m rail)
[9] For "Load deflection test".
[10] For fatigue test.
[11] Only values for Classes of joint A&B are listed here.
[12] Longitudinal distance between vertical supports L_2=400 mm
[13] Actuators A&B supply a variable load in the range 5÷205 kN in counterphase. Nevertheless, the bending moment remains the same when the two forces overlap.

Figure 23. *Comparison of some national and international standards on joint acceptance tests.*

References

[1] N. K. Mandal, M. Spiryagin, Q. Wu, Z. Wen and S. Stichel: *FEA of mechanical behaviour of insulated rail joints due to vertical cyclic wheel loadings*, Engineering Failure Analysis, 2022, 133.

[2] T. X. Wu, D.J. Thompson: *On the impact noise generation due to a wheel passing over rail joints*, Journal of Sound and Vibration, 2003, 267 485–496.

[3] H. Askarinejad, M. Dhanasekar, P. Boyd and R. Taylor: *Field Measurement of Wheel–Rail Impact Force at Insulated Rail Joint*, Experimental Techniques, 2015, 39 61-69.

[4] M. Quirchmair: *Optimising the track bedding stiffness and settlement behaviour at insulated rail joints*, Rail Engineering International, 2020, 4 9-14.

[5] E. Soylemez and K. Ciloglu: *Influence of track variables and product design on insulated rail joints*, Transportation Research Record: Journal of the Transportation Research Board, 2016, 2545 1-10.

[6] M. Gallou, B. Temple, C. Hardwick, M. Frost and A. El-Hamalawi: *Potential for external reinforcement of insulated rail joints*, Proc IMechE Part F: J Rail and Rapid Transit, 2018, 232(3), 697-708.

[7] N. Zong, M. Dhanasekar: *Minimization of railhead edge stresses through shape optimization*, Engineering Optimization, 2013, 45(9) 1043-1060.

[8] N. Zong, M. Dhanasekar: *Experimental studies on the performance of rail joints with modified wheel/railhead contact*, 2014, 228(8) 857-877.

[9] M. Dhanasekar: *Sleeper embedded insulated rail joints for minimising the number of modes of failure*, Engineering Failure Analysis, 2017, 76 27-43.

[10] M. Dhanasekar, W. Bayissa: *Performance of square and inclined insulated rail joints based on field strain measurements*, Proc IMechE Part F: J Rail and Rapid Transit, 2011, 226 140-155.

[11] R. H. Plaut, H. Lohse-Busch, A. Eckstein, S. Lambrecht and D. A. Dillard: *Analysis of tapered, adhesively bonded, insulated rail joints*, Proc IMechE Part F: J Rail and Rapid Transit, 2007 221-195.

[12] prEN16843:2019: *Railway applications - Infrastructure – Mechanical requirements for joints in running rails*, CEN, Brussels, 2019.

[13] Italian Patent 102022000009896, 12.05.2022

[14] EN13674-2:2019: *Railway applications - Track - Rail - Part 2: Switch and crossing rails used in conjunction with Vignole railway rails 46 kg/m and above*, CEN, Brussels, 2019.

[15] J. Sandström and A. Ekberg: *Numerical study of the mechanical deterioration of insulated rail joints*, Proc IMechE Part F: J Rail and Rapid Transit, 2009, 223 265-273.

[16] N. K. Mandal: *FEA to assess plastic deformation of rail head material damage of insulated rail joints with fibre glass and nylon end posts*, Wear, 2016, 366-367 3-12.

[17] N. K. Mandal, M. Dhanasekar and Y. Quan Sun: *Impact forces at dipped rail joints*, Proc IMechE Part F: J Rail and Rapid Transit, 2016, 230(1) 271-282.

[18] H.H. Jenkins, J.E. Stephenson, G.A. Clayton, et al: *The effect of track and vehicle parameters on wheel/rail vertical dynamic forces*. Railway Engineering Journal, 1974, 3(1) 2–16.

[19] I. Grossoni, S. Iwnicki, Y. Bezin and C. Gong: *Dynamics of a vehicle–track coupling system at a rail joint*, Proc IMechE Part F: J Rail and Rapid Transit, 2015, 229(4) 364-374.

[20] A.A. Shabana, M. Berzeri and J.R. Sany: *Numerical Procedure for the Simulation of Wheel/Rail Contact Dynamics*, J. Dyn. Sys. Meas. Control, 2001, 123(2) 168-178

[21] N. Bosso, A. Bracciali, G. Megna, N. Zampieri: *Effects of geometric track irregularities on vehicle dynamic behaviour when running through a turnout*, Vehicle System Dynamics, DOI: 10.1080/00423114.2021.1957127, published online: 30 July 2021.